ACS APPLIED MATERIALS & INTERFACES

Letter

www.acsami.org

Low-Cost Synthesis of Hierarchical V_2O_5 Microspheres as High-Performance Cathode for Lithium-Ion Batteries

Jie Shao, Xinyong Li, Zhongming Wan, Longfei Zhang, Yuanlei Ding, Li Zhang, Qunting Qu,* and Honghe Zheng*

School of Energy & College of Chemistry, Chemical Engineering and Material Science, Soochow University, Suzhou Jiangsu 215006, China

Supporting Information

ABSTRACT: Hierarchical V_2O_5 microspheres composed of stacked platelets are fabricated through a facile, low-cost, and energy-saving approach. The preparation procedure involves a room-temperature precipitation of precursor microspheres in aqueous solution and subsequent calcination. Because of this unique structure, V_2O_5 microspheres manifest a high capacity (266 mA h g^{-1}), excellent rate capability (223 mA h g^{-1} at a current density 2400 mA g^{-1}), and good cycling stability (200 mA h g^{-1} after 100 cycles) as cathode materials for lithium-ion batteries.

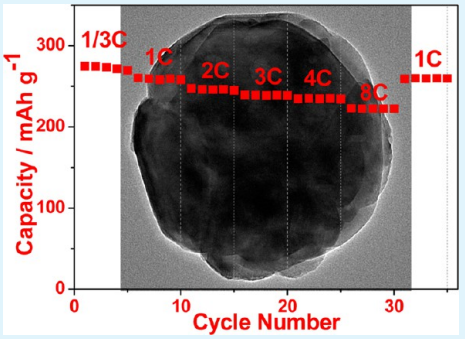

KEYWORDS: *cathode, Li-ion batteries, microspheres, vanadium pentoxide*

1. INTRODUCTION

Lithium-ion batteries are the predominant power sources for the current portable electronics. However, their energy and power density, largely depending on the electrochemical properties of electrode materials, still cannot meet the aggressive demands of electric vehicles (EVs) and hybrid electric vehicles (HEVs).[1−5] In addition, commercial lithium ion batteries suffer from the specific capacity mismatch between cathode and anode materials. As summarized in Figure 1a, the practical reversible capacities of typical commercial cathodes (usually less than 190 mA h g^{-1})[2,6−8] are far lower than that of graphite anode (372 mA h g^{-1}). This is known as an important reason for the low energy density of various kinds of full cells. From this point of view, exploration of alternative cathode materials of higher capacity is essential for developing next-generation of high-energy and high-power lithium-ion batteries.[9]

V_2O_5, because of its high theoretical capacity (294 mA h g^{-1} based on two lithium insertion per formula unit), high output voltage, abundant resource, and lost cost, has been considered as a promising cathode for lithium-ion batteries.[10−13] Especially, nanostructured V_2O_5, such as nanotubes,[14] nanoparticles,[12,15] nanowires,[16,17] and mesoporous materials,[18] have demonstrated superior lithium insertion/extraction performances. Nonetheless, the associated problems, like low packing density and high reactivity of electrolyte at the electrode surface, always lead to the low volumetric energy density, poor cycling stability, and safety hazards of the battery.[19−21] Fabrication of hierarchical microspheres composed of nanostructures provides a feasible strategy to overcome these limitations.[21] As a matter of fact, hierarchical hollow V_2O_5 microspheres,[11,22] porous V_2O_5 microspheres,[23,24] and yolk−shell V_2O_5 microspheres[10,25,26] have been reported with much improved lithium storage properties. However, preparation of these microspheres always involve a two-step heat treatment (solvothermal step and calcination step), which are time- and energy-consuming.[10,22,23,25−29] Besides, the adopted solvent and vanadium sources are always quite expensive.

In this work, we present a novel facile and low-cost approach to fabricate hierarchical V_2O_5 submicrospheres composed of stacked platelets. The preparation procedure involves a room-temperature precipitation of $V(OH)_2NH_2$ precursor in aqueous solution and subsequent calcination. Diameter of the V_2O_5 microspheres is well controllable by adjusting the composition of precursor solution. The obtained V_2O_5 microspheres manifest excellent electrochemical performance as cathode materials for lithium-ion batteries.

2. RESULTS AND DISCUSSION

The detailed preparation procedures of V_2O_5 microspheres are shown in the Experimental Section. Briefly, the $V(OH)_2NH_2$ precursor was first prepared as previously reported, which is based on a precipitation reaction of NH_4VO_3, HCl, and hydrazine-containing aqueous solution at room-temperature.[30] The precursor was subsequently calcined at 350 °C in air to obtain V_2O_5. The crystal phases of precursor and V_2O_5 were

Received: May 16, 2013
Accepted: August 5, 2013
Published: August 5, 2013

   dx.doi.org/10.1021/am401854v | ACS Appl. Mater. Interfaces 2013, 5, 7671−7675

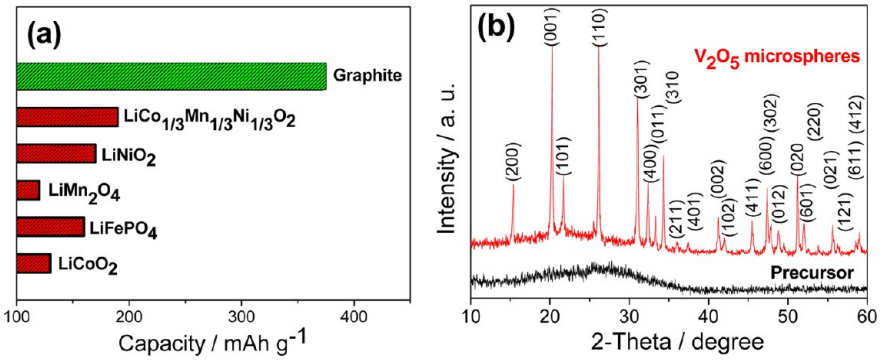

Figure 1. (a) Practical reversible capacities of some typical commercial cathodes and graphite anode. (b) XRD patterns of the precursor and as-prepared V_2O_5 microspheres.

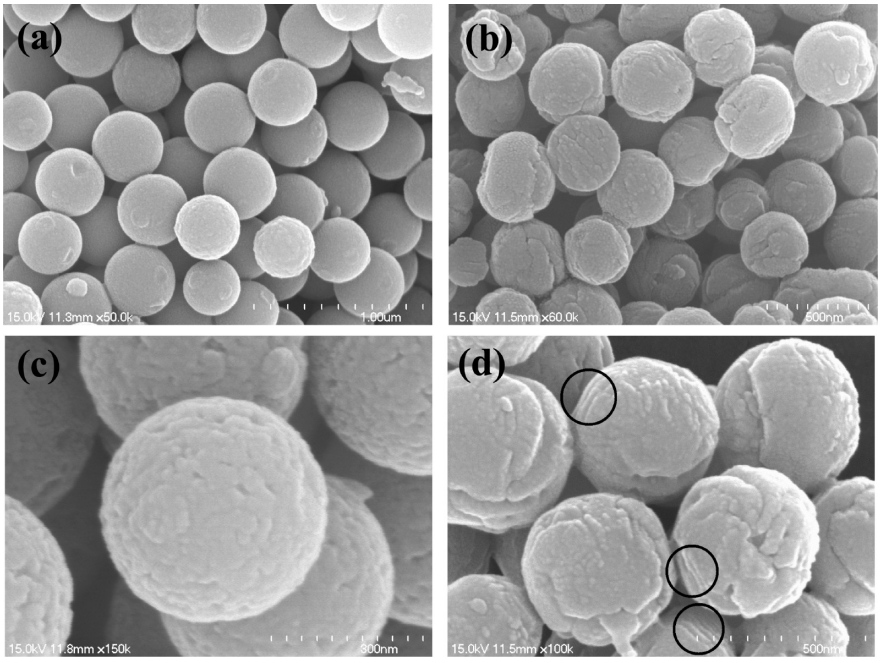

Figure 2. SEM images of the (a, c) precursor and (b, d) as-prepared V_2O_5 microspheres at different magnifications.

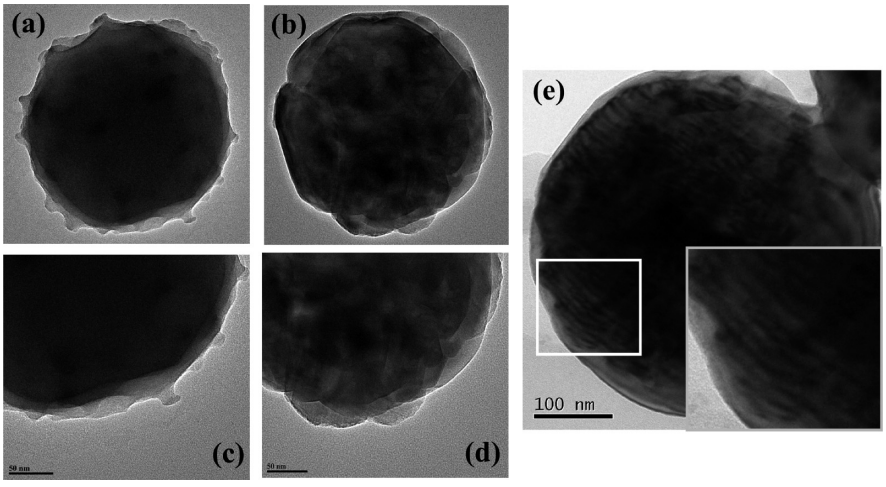

Figure 3. TEM images of the (a, c) precursor and (b, d, e) as-prepared V_2O_5 microspheres. The inset in e is the magnification of rectangular region.

investigated by X-ray diffraction (XRD) patterns (Figure 1b). The precursor exhibits an amorphous structure. After calcinations at 350 °C, it converts into crystalline V_2O_5. All the diffraction peaks can be indexed to orthogonal V_2O_5 phase (α-V_2O_5, JCPDF no. 41−1426). Thermogravimetric (TG) curve of $V(OH)_2NH_2$ precursor (Figure S1 in the Supporting

dx.doi.org/10.1021/am401854v | ACS Appl. Mater. Interfaces 2013, 5, 7671−7675

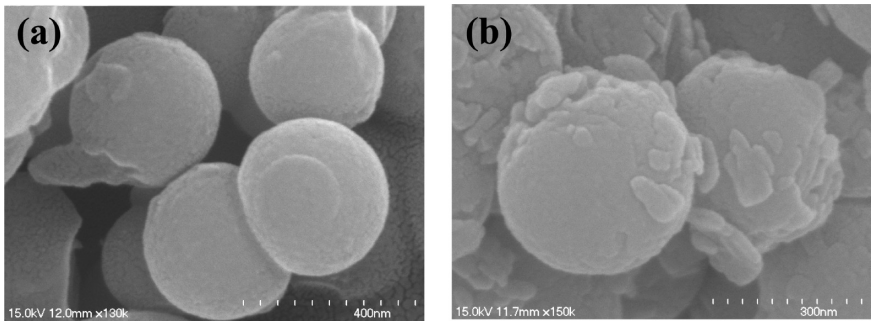

Figure 4. SEM images of the (a) precursor and (b) V_2O_5 microspheres prepared in presence of formic acid in the precursor solution.

Information) under air atmosphere displays a mass loss of 9% between 50 and 350 °C, which is a combined effect of water and NH_3 release and oxidization of V^{3+} by oxygen. No more weight loss is observed at temperature above 350 °C. The as-prepared V_2O_5 is thermally stable in the whole range of detected temperature, suggesting that the precursor is completely converted into V_2O_5 at 350 °C.

Morphologies of the samples were studied using scanning electron microscopy (SEM). Figure 2a reveals that the original precursor is composed of homogeneous microspheres with diameter of about 400 nm. After calcination at 350 °C for 2h, the original microspherical morphology and size is well maintained (see Figure 2b). It is noteworthy that the as-prepared V_2O_5 submicrospheres are much smaller than the microscaled spheres reported in literatures.[10,25,28] This is associated with the small dimension of precursor microspheres synthesized at room-temperature. The precursors in literatures are always prepared via a solvothermal step at high temperature, leading to aggregation of nanomaterials and growth of microspheres to a larger size. The high-rate SEM images of precursor and V_2O_5 (Figure 2c, 2d) reveal that these microspheres consist of platelike structure. Especially, for the V_2O_5 microspheres, the layer-by-layer edges of plates can be observed distinctly as marked out in the circle regions.

Transmission electron microscopy (TEM) was further utilized to confirm the hierarchical structure of these microspheres. By comparing the TEM images of precursor and V_2O_5 microspheres (Figure 3a, b), we can see that the precursor presents a very dense structure. In contrast, the interior of V_2O_5 microspheres is considerably looser than the precursor. This is believed to be resulted from the water and NH_3 release during thermal decomposition of the $V(OH)_2NH_2$ precursor. A deep insight into the edges of precursor and V_2O_5 microspheres (Figure 3c, d) shows that these materials seem to be composed of stacked platelets, consistent with the above SEM results. Especially, one typical side-view image of V_2O_5 microspheres presents well-ordered stacking of layer-by-layer structure (Figure 3e). Brunauer–Emmett–Teller (BET) specific surface area of V_2O_5 microspheres measured through nitrogen adsorption/desorption isotherms (see Figure S2 in the Supporting Information) is 12 m^2 g^{-1}, validating presence of pores or interstices between the primary platelets of V_2O_5 microspheres. The pore size distribution curve shows broadly distributed mesopores with diameters below 50 nm.

Diameter of the precursor and V_2O_5 microspheres can be well controlled by adjusting the pH environment of the precursor solution. When 1 mL of formic acid is introduced into the reaction solution, diameter of the precursor and resultant V_2O_5 microspheres is decreased to 300 nm (Figure 4). This may be related to the high sensitivity of $V(OH)_2NH_2$ precursor to H^+ ions, and thus the outer layer of $V(OH)_2NH_2$ microspheres may dissolve into the solution. By contrast, influence of calcination time on the morphologies of V_2O_5 microspheres is negligible (Figure S3 in the Supporting Information). Here it also should be pointed out that SEM image of some collapsed V_2O_5 microspheres (Figure 4b) contains rubblelike platelets, further suggesting that this material should be composed of platelike structure.

A schematic is shown in Scheme 1 to illustrate the formation of hierarchical structured V_2O_5 microspheres. The V-

Scheme 1. Schematic Illustration of the Formation of Precursor and Hierarchical V_2O_5 Microspheres from the Side View

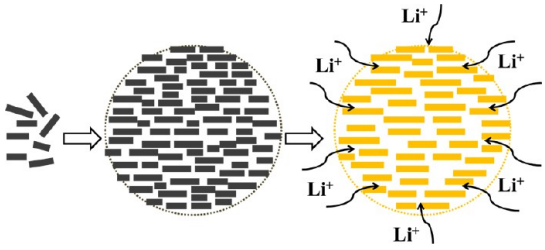

$(OH)_2NH_2$ precursors are first generated in the form of plate-like structure by the redox reaction between VO_3^- and hydrazine, which then aggregated or stacked to form solid microspheres during the aging process. After calcination, V_2O_5 microspheres with a looser interior are achieved due to release of water and NH_3. As observed from the SEM images of precursor and V_2O_5 at high magnification (Figure 2c, d), dimensions of these primary platelets increase slightly after heat treatment, probably due to the agglomerative growth of V_2O_5 plates during calcination. This work provides a novel route for the fabrication of hierarchical V_2O_5 submicrospheres assembled from stacked platelets. Compared with other reports involving a two-step heat treatment,[10,22,23,25−29] this method is more facile, scalable, low-cost, and energy-saving, making it suitable for industrial application.

Figure 5a shows the cyclic voltammograms (CV) of the V_2O_5 submicrospheres electrode within the voltage range of 2−4 V vs Li/Li^+. This voltage window is chosen to avoid the formation of irreversible ω-phase of $Li_xV_2O_5$ ($2 < x < 3$) that occurs at deep depth of discharge. The three cathodic peaks at the potentials of 3.34, 3.13, and 2.21 V are attributed to the formation of intercalation compounds ε-$Li_{0.5}V_2O_5$, δ-LiV_2O_5, and γ-$Li_2V_2O_5$, respectively.[10] The corresponding anodic peaks at the potentials of 2.59, 3.28, and 3.47 V due to lithium

dx.doi.org/10.1021/am401854v | ACS Appl. Mater. Interfaces 2013, 5, 7671−7675

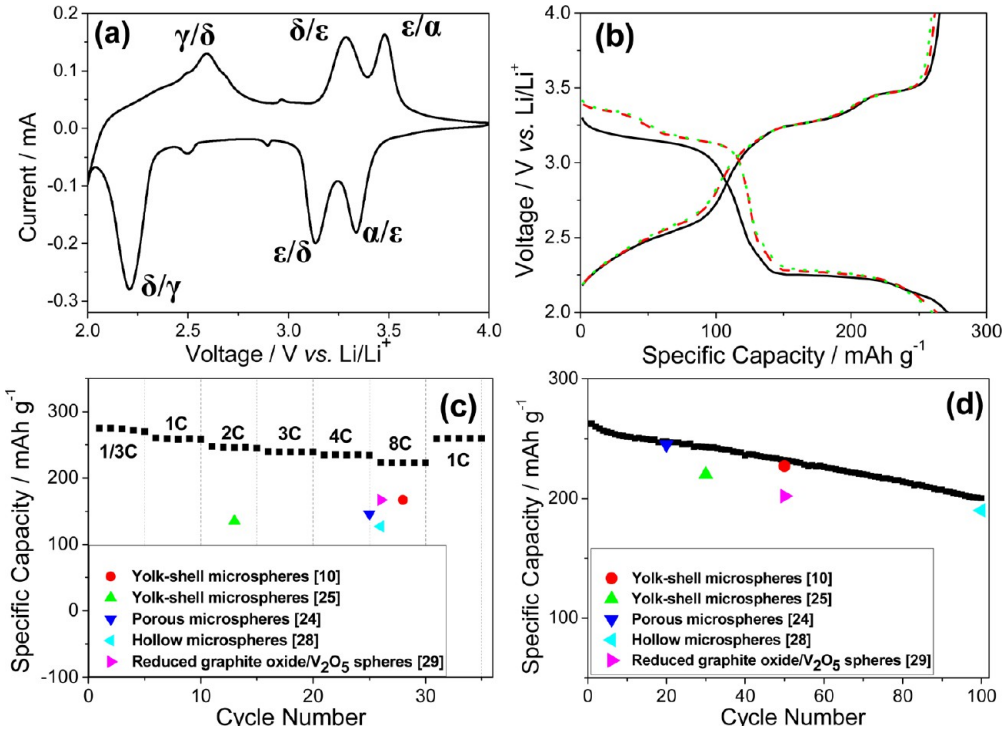

Figure 5. (a) CV curve of V_2O_5 microsphere electrode. (b) Galvanostatic discharge and charge curves of V_2O_5 electrode at a current density of 300 mA g^{-1} (1C); first cycle (—), second (---), and third (●●●) cycle. (c) Rate performance of V_2O_5 microsphere electrode and the comparison with the reported results at the corresponding rate. (d) Long-term cycling performance of V_2O_5 microspheres during discharge/charge at a current rate of 1C, and the comparison with other reported results at the corresponding cycle number.

deintercalation signify the backward transition of phases from γ-$Li_2V_2O_5$ to δ-$Li_{0.5}V_2O_5$, ε-LiV_2O_5, and α-V_2O_5, respectively.[10]

The galvanostatic discharge and charge curves of V_2O_5 electrode at a current density of 300 mA g^{-1} (1C) are presented in Figure 5b. During discharge, well-defined voltage plateaus appear at 3.34, 3.15, and 2.25 V, representing the multiple-step lithium ion intercalation. Deintercalation of lithium ions also occurs in three steps, consistent with the above CV results. The Coulombic efficiencies for the initial three cycles are 97.8, 99.6, and 99.9%, respectively, signifying excellent reversibility of V_2O_5 microspheres electrodes for the insertion/extraction of lithium ions. A reversible capacity of 266 mA h g^{-1}, close to the theoretical capacity of 294 mA h g^{-1}, is obtained in the initial cycle. The specific capacity of V_2O_5 microspheres is significantly higher than those of porous microspheres (214 mA h g^{-1}),[24] yolk-shell microspheres (180 mA h g^{-1}),[25] hollow microspheres (241 mA h g^{-1}),[28] and three-dimensional porous V_2O_5[31] (230 mA h g^{-1}) tested at similar current rate.

Rate capability test of the V_2O_5 microspheres (Figure 5c) demonstrates a reversible capacity of 223 mA h g^{-1} at 8C (equivalent to 2400 mA g^{-1}), considerably higher than those of porous,[24] hollow[28] or yolk−shell V_2O_5[10,25] microspheres and even reduced graphene oxide supported V_2O_5 spheres[29] reported previously under similar test conditions. The improved rate performance of V_2O_5 microspheres can be attributed to their hierarchical microspherical structures assembled from primary platelets. On the one hand, the interstices between these primary platelets facilitate intercalation of lithium ions from various directions of the spheres (Scheme 1). On the other hand, dimension of the present V_2O_5 microspheres with a uniform diameter of 400 nm is much smaller than those reported in literature (usually larger than 1 μm),[10,25,28] which ensures fast Li^+ transportation throughout the particles.

Cycling stability of the V_2O_5 microspheres during long-term discharge/charge at a current rate of 1C is shown in Figure 5d. The specific capacity at the 20th, 50th, and 100th cycle is 248, 232, and 200 mA h g^{-1}, respectively. The capacity retention of V_2O_5 microspheres is superior to those of hollow and yolk-shell V_2O_5 microspheres reported in literatures[10,24,25,28,29] with the same voltage window applied. The interstices between the primary plates can effectively alleviate the volume expansion/contraction of V_2O_5 upon cycling. The secondary microspherical structure could suppress aggregation of the primary platelets. In other words, the hierarchical structure of V_2O_5 microspheres accounts for its good cycling performance. Considering that there is no Li in V_2O_5, practical application of V_2O_5 can be extended to metal lithium batteries, in which the problem of Li dendrites could be resolved through utilization of high salt concentration electrolytes.[32]

3. CONCLUSION

In conclusion, a facile and low-cost approach was developed for the synthesis of hierarchical V_2O_5 microspheres composed of stacked platelets. V_2O_5 microspheres manifest a reversible capacity of 266 mA h g^{-1} at a current rate of 1C. The V_2O_5 microspheres also exhibit excellent high-rate capability and good cycling stability attributed to the unique hierarchical structure of V_2O_5 material. The new synthesis process for such hierarchical V_2O_5 microspheres adopted in this study is scalable and energy-saving, making it a promising cathode material for the next-generation of high-energy lithium-ion or lithium batteries.

■ ASSOCIATED CONTENT

Supporting Information

Experimental details, TG curves of $V(OH)_2NH_2$ precursor and as-prepared V_2O_5 microspheres under air atmosphere, N_2 adsorption−desorption isotherms and corresponding pore size distribution curves of V_2O_5 microspheres, TEM images of V_2O_5 microspheres prepared through different calcination time, and charge curves of the V_2O_5 microspheres at different current rates. This material is available free of charge via the Internet at http://pubs.acs.org.

■ AUTHOR INFORMATION

Corresponding Author

*E-mail: qtqu@suda.edu.cn (Q.Q.); hhzheng@suda.edu.cn (H.Z.).

Author Contributions

The manuscript was written through contributions of all authors. All authors have given approval to the final version of the manuscript.

Notes

The authors declare no competing financial interest.

■ ACKNOWLEDGMENTS

This work was supported by National Natural Science Foundation of China (NSFC 21203133 and 51272168) and The Natural Science Foundation of Jiangsu Province (BK2012186).

■ REFERENCES

(1) Whittingham, M. S. *Chem. Rev.* **2004**, *104*, 4271−4302.
(2) Kang, B.; Ceder, G. *Nature* **2009**, *458*, 190−193.
(3) Bruce, P. G.; Scrosati, B.; Tarascon, J.-M. *Angew. Chem., Int. Ed.* **2008**, *47*, 2930−2946.
(4) Armand, M.; Tarascon, J. M. *Nature* **2008**, *451*, 652−657.
(5) Shao, J.; Li, X.; Zhang, L.; Qu, Q.; Zheng, H. *Nanoscale* **2013**, *5*, 1460−1464.
(6) Wang, Y.; Cao, G. *Adv. Mater.* **2008**, *20*, 2251−2269.
(7) Qu, Q.; Fu, L.; Zhan, X.; Samuelis, D.; Maier, J.; Li, L.; Tian, S.; Li, Z.; Wu, Y. *Energy Environ. Sci.* **2011**, *4*, 3985−3990.
(8) Devaraju, M. K.; Honma, I. *Adv. Energy Mater.* **2012**, *2*, 284−297.
(9) Kraytsberg, A.; Ein-Eli, Y. *Adv. Energy Mater.* **2012**, *2*, 922−939.
(10) Pan, A.; Wu, H. B.; Yu, L.; Lou, X. W. *Angew. Chem., Int. Ed.* **2013**, *52*, 2226−2230.
(11) Cao, A.-M.; Hu, J.-S.; Liang, H.-P.; Wan, L.-J. *Angew. Chem., Int. Ed.* **2005**, *44*, 4391−4395.
(12) Hu, Y.-S.; Liu, X.; Müller, J.-O.; Schlögl, R.; Maier, J.; Su, D. S. *Angew. Chem., Int. Ed.* **2009**, *48*, 210−214.
(13) Zhang, X.-F.; Wang, K.-X.; Wei, X.; Chen, J.-S. *Chem. Mater.* **2011**, *23*, 5290−5292.
(14) Wang, Y.; Takahashi, K.; Lee, K. H.; Cao, G. Z. *Adv. Funct. Mater.* **2006**, *16*, 1133−1144.
(15) Ng, S.-H.; Patey, T. J.; Buchel, R.; Krumeich, F.; Wang, J.-Z.; Liu, H.-K.; Pratsinis, S. E.; Novak, P. *Phys. Chem. Chem. Phys.* **2009**, *11*, 3748−3755.
(16) Zhai, T.; Liu, H.; Li, H.; Fang, X.; Liao, M.; Li, L.; Zhou, H.; Koide, Y.; Bando, Y.; Golberg, D. *Adv. Mater.* **2010**, *22*, 2547−2552.
(17) Mai, L.; Xu, L.; Han, C.; Xu, X.; Luo, Y.; Zhao, S.; Zhao, Y. *Nano Lett.* **2010**, *10*, 4750−4755.
(18) Yu, D.; Chen, C.; Xie, S.; Liu, Y.; Park, K.; Zhou, X.; Zhang, Q.; Li, J.; Cao, G. *Energy Environ. Sci.* **2011**, *4*, 858−861.
(19) Sun, Y.-K.; Oh, S.-M.; Park, H.-K.; Scrosati, B. *Adv. Mater.* **2011**, *23*, 5050−5054.
(20) Xiang, H. F.; Wang, H.; Chen, C. H.; Ge, X. W.; Guo, S.; Sun, J. H.; Hu, W. Q. *J. Power Sources* **2009**, *191*, 575−581.
(21) Jung, H.-G.; Myung, S.-T.; Yoon, C. S.; Son, S.-B.; Oh, K. H.; Amine, K.; Scrosati, B.; Sun, Y.-K. *Energy Environ. Sci.* **2011**, *4*, 1345−1351.
(22) Pan, A.; Zhu, T.; Wu, H. B.; Lou, X. W. *Chem.—Eur. J.* **2013**, *19*, 494−500.
(23) Zhang, C.; Chen, Z.; Guo, Z.; Lou, X. W. *Energy Environ. Sci.* **2013**, *6*, 974−978.
(24) Wang, S.; Lu, Z.; Wang, D.; Li, C.; Chen, C.; Yin, Y. *J. Mater. Chem.* **2011**, *21*, 6365−6369.
(25) Liu, J.; Zhou, Y.; Wang, J.; Pan, Y.; Xue, D. *Chem. Commun.* **2011**, *47*, 10380−10382.
(26) Pang, H.; Cheng, P.; Yang, H.; Lu, J.; Guo, C. X.; Ning, G.; Li, C. M. *Chem. Commun.* **2013**, *49*, 1536−1538.
(27) Liu, J.; Xia, H.; Xue, D.; Lu, L. *J. Am. Chem. Soc.* **2009**, *131*, 12086−12087.
(28) Uchaker, E.; Zhou, N.; Li, Y.; Cao, G. *J. Phys. Chem. C* **2013**, *117*, 1621−1626.
(29) Rui, X.; Zhu, J.; Sim, D.; Xu, C.; Zeng, Y.; Hng, H. H.; Lim, T. M.; Yan, Q. *Nanoscale* **2011**, *3*, 4752−4758.
(30) Wu, C.; Zhang, X.; Ning, B.; Yang, J.; Xie, Y. *Inorg. Chem.* **2009**, *48*, 6044−6054.
(31) Wang, S.; Li, S.; Sun, Y.; Feng, X.; Chen, C. *Energy Environ. Sci.* **2011**, *4*, 2854−2857.
(32) Suo, L.; Hu, Y.; Li, H.; Armand, M.; Chen, L. *Nat. Commun.* **2013**, *4*, 1481.